Journal of the Korean Physical Society, Vol. 53, No. 2, August 2008, pp. 990∼994

Direct Mapping of Magnetoresistance to Magnetic Domain Image in Permalloy Thin Films by Simultaneous Measurement

Dong Ho KIM* and Tae-Jong HWANG†
Department of Physics, Yeungnam University, Gyeongsan 712-749

Kwang-Su RYU and Sung-Chul SHIN
Department of Physics and Center for Nanospinics of Spintronic Materials, Korea Advanced Institute of Science and Technology, Daejeon 305-701

(Received 21 August 2007)

We report the first simultaneous measurements of the magnetoresistance (MR) and the magnetic domain images in two-dimensional permalloy thin films by utilizing a magneto-optic magnetic microscope. In this way, we could directly map the MR to the domain patterns without any ambiguity. For 30-nm-thick permalloy films with in-plane uniaxial magnetization, negative MR was observed when the domain wall was nucleated. An analysis of the MR change with the anisotropic magnetoresistance resulted in a rather large domain wall thickness of 1.7 μm compared to the well-known theoretical value of 0.3 μm. We discuss possible origins of this discrepancy in terms of wide domain tails, wavy domain boundaries, and intrinsic properties associated with permalloy. This new method can be utilized to investigate the magnetic properties of newly emergent materials.

PACS numbers: 75.60.Ch, 75.50.Bb
Keywords: Magnetoresistance, Domain patterns, Domain wall resistance

I. INTRODUCTION

One interesting topic in magnetic transport properties is the resistance of magnetic domain walls (DWs) in ferromagnetic (FM) materials. A DW is a surface that separates the magnetic domains and over which the orientation of the magnetic moment changes abruptly. Electrons travelling in one domain will experience a different potential when entering an oppositely magnetized domain due to a band minimum difference caused by exchange energy splitting. The presence of the DW, then, can be simply modelled as a potential barrier in the way of current path. When the DW is abrupt compared to the Fermi wavelength (0.1 nm), lower transmission of electrons results in domain-wall resistance (DWR). For wall thickness much larger than the Fermi wavelength, the resistance change can be quite small. The search for the DWR has been a quite interesting topic experimentally as well as theoretically in recent years [1]. A detailed quantum mechanical estimate of the DWR, which predicts a positive DWR, has been put forward by Levy and Zhang; they considered a spin mistracking effect in rotating exchange field inside the DW [2]. On the other hand, Tatara and Fukuyama pointed out that spatially inhomogeneous magnetization in a DW can destroy the weak localization effect resulting in a decrease in the DWR, which can dominate over the conventional resistivity [3].

The difficulty in determing the DWR arises from the presence of other magnetoresistance (MR) effects, such as anisotropic magnetoresistance (AMR) [4] from the domain, whose contribution to the total resistance is much larger than that of the DWR since the fractional volume of the DW is very small. To obtain more precise results, studies on well-defined geometry having an isolated domain wall have been extensively performed. Experimental reports on the DWR vary from a decrease to an increase in the resistance. For instance, a positive DWR has been observed in the nanowires of a Co/Pt multilayer with out-of-plane anisotropy, where the current is always perpendicular to the magnetization, including the Bloch domain wall [5]. In that way, the AMR contribution from the DW can be eliminated. In a FePd nanostructure, a positive DWR was also observed [6]. On the other hand, a negative DWR has been detected in Fe [7], Ni [8], and permalloy nanowires [9]. There are other reports that emphasize the spin accumulation effect at the wall [10] or the role of the AMR from the Neel cap in Bloch walls [11], or effects of reduced surface scattering near the wall on the DWR [12]. In order to clarify the MR results, the domain images of the corresponding samples have been taken mostly by using magnetic force microscope [5–7,

*E-mail: dhkim@ynu.ac.kr;
†Fax: +82-53-810-4613

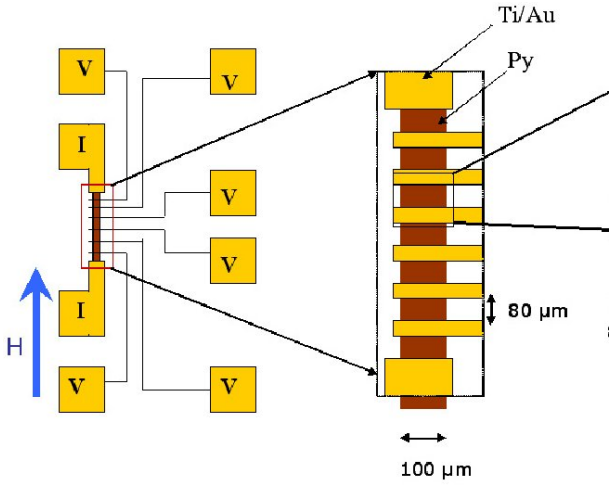

Fig. 1. A schematic diagram of the patterned sample and a real image are shown. The square in the real image denotes the field of view of the MOMM.

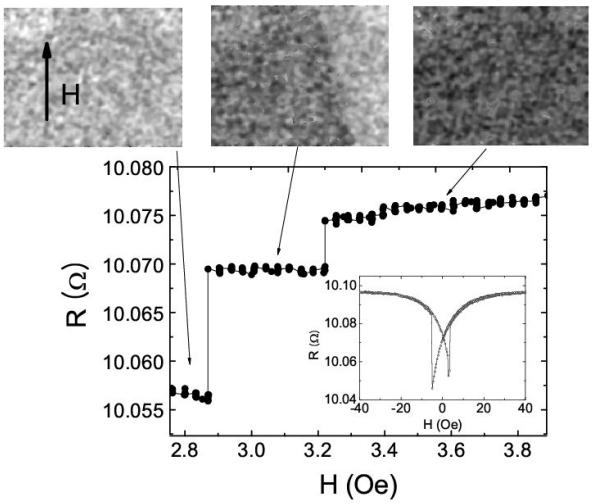

Fig. 2. The simultaneously-obtained domain patterns and their MR for sample P30, whose magnetization easy axis is inclined 30° from the strip direction, are shown. The inset displays the hysteretic MR changes of P30 during one complete H sweep. A sharp MR change appeared when a domain wall was nucleated.

10,12] and have been compared with the transport properties. However, all those previous measurements of the domain patterns and the MR have been performed separately or nucleation of the DW has inferred from the transport data.

In this work, we adopt a new experimental scheme that measures the MR and the domain patterns of FM materials simultaneously, which is capable of direct mapping the MR changes to the domain evolutions. In this way, we could reduce the ambiguity that might take place when interpreting the MR data in terms of domain resistance and domain-wall resistance.

II. EXPERIMENTS

Permalloy (Py:$Ni_{80}Fe_{20}$) thin films were used for the FM material because the magnetic properties of Py have been intensively studied for many years and are well known [13]. To ensure the Néel-type domain walls, we grew a 30-nm thick Py layer on a SiO_2/Si substrate at a water-cooled temperature by dc magnetron sputtering, and we deposited a 5-nm-thick non-magnetic Nb cap layer subsequently on top of the Py layer to prevent oxidation. The orientation of the magnetization easy axis was defined by the residual magnetic field in the growth chamber and was later determined by measuring the hysteresis loops while rotating the sample in an external field. In this way, we found that the as-grown Py layers were uniaxially magnetized, and we could determine the orientation of the magnetization easy axis within uncertainty of 5°.

We utilized a magneto-optic microscope magnetometer (MOMM) to simultaneously measure the MR and the domain patterns. The magnet on the sample stage of the MOMM could generate magnetic field (H) up to 1 kOe in a direction parallel to the film plane. The Py film was first patterned in a rectangular shape of 100 μm × 670 μm by using photolithography and Ar-ion milling. Ti/Au electrodes were prepared for current and voltage contacts by using the lift-off method. The area between two voltage contacts was 100 μm × 80 μm, and the field of view of the MOMM was 80 μm × 64 μm. We positioned the sample so that the field of view was between the edges and voltage contacts to avoid unwanted background reflections from the metal surface and the sample stage. The schematic shape of the patterned sample and the real image are shown in Figure 1. Also shown is the direction of the in-plane H. For the measurements, the in-plane magnetization (M) was first saturated by applying a negative saturation field along the strip axis; then, the H was ramped down to zero, reversed, and ramped up to a field just below the positive coercive field (H_c) where the magnetization switching occurs. From this point, the H was slowly ramped up crossing H_c while the MR measurement by using a four-terminal dc method and the frame grabbing of the domain patterns by using the MOMM were simultaneously performed.

III. RESULTS AND DISCUSSION

The first sample, P30, has its magnetization easy axis inclined 30° from the long axis of the strip. Figure 2 shows the simultaneously-obtained domain patterns and their MR. The external field was applied along the vertical direction of the images as denoted in the figure, which is along the strip axis. The inset shows the hysteretic MR behavior of P30 during a complete cycle of the H sweep.

Before we look into the details of M switching, we need to understand the general behavior of the MR during one H cycle. The MR gradually decreases from the saturation value until a sudden increase of MR along with magnetization switching occurs. The gradual decrease in the MR can be explained in terms of AMR, where the resistivity of the magnetization parallel to the current ($\rho_{\|}$) is greater than that of the magnetization perpendicular to the current ($\rho_{\perp}$) due to the spin-orbit coupling [4]. The AMR effect can be given in the following equation:

$$\rho_{AMR} = \rho_{\perp} + [\rho_{\|} - \rho_{\perp}] \cos^2 \theta, \quad (1)$$

where θ is the angle between the magnetization and the current. At saturation, where the magnetization is forced to align parallel to the external field, which is in the same direction as that of the bias current, the MR has its highest value. On decreasing H, the magnetic moment rotates away from the long axis toward the easy axis such that the MR is reduced according to Eq. (1) as θ is increased. The jump of the MR at H_c is related to the magnetization switching. The main panel shows a magnified view of the MR jump during the magnetization reversal process. The corresponding domain patterns are also shown in Figure 2. The white and the black regions of the images indicate the domains just before and after switching, respectively. The MR shows a stepwise increase with increasing H, and the step is clearly associated with nucleation of the domain wall. However, since the MRs of the two white and black domains in Figure 2 are different due to the AMR effect, it is quite difficult to quantify the DWR contribution. Thus, we performed the same measurement on the samples with their easy axes aligned almost parallel to the current direction. In this case, the MRs of the two domain states before and after the magnetization switching are the same so that the MR change can be solely related to the effect of the DW.

Figure 3 shows a typical domain evolution and its corresponding MR and Kerr intensity for sample P01 with its easy axis oriented along the current direction. The MR showed a sudden decrease when a 180° DW nucleated, and the reduced MR was maintained until the completion of the magnetization switching. The arrows indicate the magnetizations of the domains. This result clearly demonstrates that the observed MR change is directly related to DW nucleation, as also evidenced by the simultaneous sudden changes in the Kerr intensity and the MR. For permalloy, the domain wall resistance was found to be negative, similar to the previous work on permalloy [9]. The relative resistance change due to the DW in Figure 3 is around 1×10^{-4}, but this number should be multiplied by a factor of 3.3 after correcting for the shunt resistance effect due to the Nb capping layer. The correction was made by measuring the resistivities of single Nb and Py layers and the thickness of each layer of the Py/Nb samples.

There is a microscopic model by Tatara and Fukuyama [3], as described earlier, that quantum interference effects give rise to a decrease in the DWR, but this effect is limited to the low-temperature region. One alternative explanation involves the AMR. In our geometry of the Néel wall, it is certain that there is a region inside the wall where the current and the local magnetization are perpendicular. Since $\rho_{\|} > \rho_{\perp}$ due to the AMR effect, the resistance of the DW is lower than that of the domains. The magnitude of the AMR can be easily obtained by measuring the resistance at the transverse saturation field and subtracting the longitudinal resistance at the saturation field from the former. In the transverse configuration with H oriented along the hard axis, magnetization reversal takes place through magnetization rotation, and the corresponding MR is known to have the shape of a parabola as a function of H [14] and could be well fit to Eq. (1) [15].

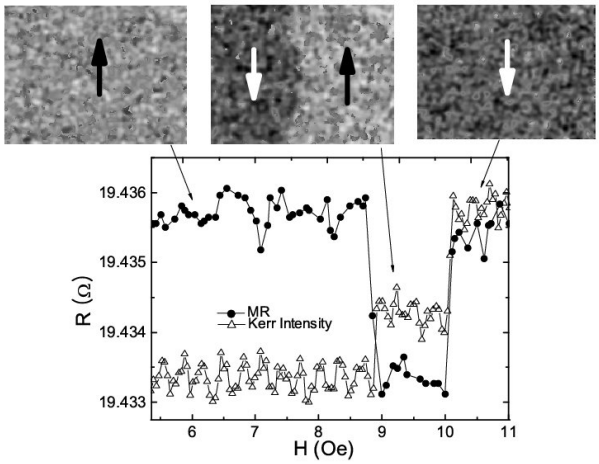

Fig. 3. A typical domain evolution and its corresponding MR and Kerr intensity of sample P01, whose easy axis is oriented along the strip direction. The MR showed a sudden decrease when a 180° DW was nucleated and the negative MR during in presence of the DW. The arrows indicate the magnetizations of the domains. This result clearly demonstrates that the observed negative MR change is directly related to DW nucleation.

In order to quantify the contribution of DW to the MR, we first assumed the AMR to be the main cause for the MR decrease. Then, the MR change observed in the experiment (ΔR_e) could be simply given by the product of the expected resistance change of the sample due to the AMR (ΔR_{AMR}) and the fractional volume ratio occupied by the DW:

$$\Delta R_e = 0.6 \Delta R_{AMR} \frac{\delta_W}{W} \frac{L_W}{L} \quad (2)$$

where δ_W is the DW thickness, and L_W is the DW length, W and L are the width and the length of the resistance-measuring area, respectively. Since the local magnetic moment in the wall rotates 180° and the AMR is proportional to $\cos^2\theta$, the effective DWR should be multiplied by an integral of $\cos^2\theta$ over the wall thickness to include the effect of a smooth variation of θ. For obtain-

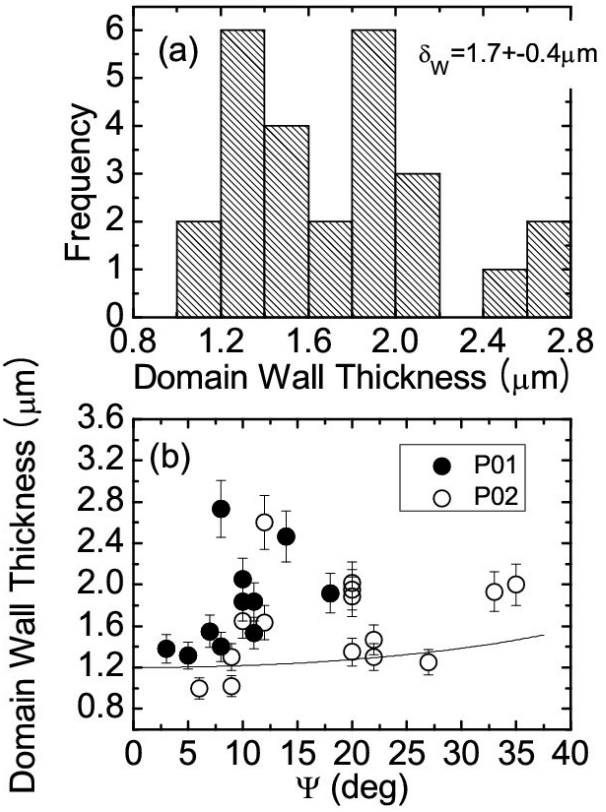

Fig. 4. (a) Distribution of the domain wall thicknesses of samples P01 and P02 obtained by assuming that the AMR effect accounted for all the MR change. (b) A plot of the DW thickness as a function of the DW inclination angle. The error bars reflect the measurement errors in determining ΔR_e. The solid line represents the $1/\cos\Psi$ dependence.

ing Eq. (2), we used the hyperbolic tangent function, $\tanh(\pi x/\delta_w)$, for the domain wall profile, where x is the distance from the center of the DW.

Now the effective domain wall thickness can be estimated from Eq. (2). When using Eq. (2), we don't need to consider the shunt effect due to the Nb layer because both ΔR_e and ΔR_{AMR} are measured with the same shunt. ΔR_{AMR}, the difference between resistances at longitudinal and transverse saturation fields, of P01 turned out to be 0.31 ohm, for instance. With this value, the effective DW thickness from 11 patterns of P01 and 15 patterns of P02, a similarly prepared sample, was estimated as 1.7 ± 0.4 μm with a rather large spread, and its histogram is shown in Figure 4(a). During the estimate, we ignored the detailed wavy features of the boundary and simply assumed a straight domain wall. We also note that the angle Ψ that the DW makes with the long axis is not always close to zero. That is, the front of the DW is oblique. We found that Ψ varies from 0 to 35°. Figure 4(b) shows a relationship between the domain wall thickness and Ψ. Except for a few points, the DW thickness, in general, follows a $1/\cos\Psi$ dependence, as shown in the solid line. This weak angle dependence is similar to the theoretical estimate of the relationship between the DW thickness and the DW inclination angle by Hubert for obliquely charged walls [16].

The thickness of the Néel wall is given as $\pi\sqrt{2A/K}$, where A is the exchange stiffness constant and K is the anisotropy energy [13]. The latter can be obtained from the hard-axis magnetization loop. For our films, we used $A = 10^{-11}$ J/m and $K = 2{,}000$ J/m^3, and these values resulted in $\delta = 0.3$ μm, much smaller than 1.0 μm of the smallest experimental estimate in Figure 4. Even if we consider δ to represent the thickness over which the spins rotate to within about 27 percent of the domain magnetization direction, the average DW thickness of 1.7 μm is still too large when compared to the theoretical estimate. In other words, if we assume the DW thickness of our permalloy films to be the theoretical value of 0.3 μm, the observed DWR cannot be explained by the AMR effect only, and the unexplained portion of the negative DWR should have origins other than the AMR effect.

The first origin we can think of is the complex, wavy nature of the DW. Even within our resolution, the DW boundary is not straight. In this case, the effective DW length can be substantially longer than the values we used for the thickness estimate when using Eq. (2). The three data points larger than 2.4 μm in Figure 4(b) may correspond to extreme cases of wavy DW boundaries. Another possible origin for large negative DWR is the long tails of Néel walls [17]. For a symmetric Néel wall with uniaxial anisotropy, the wall can be decomposed into three parts: a sharply localized core and two wide tails, which cover a good part of total rotation. Part of the charge is concentrated in the core, and the other part of the charge is widely spread in the tail. A wider tail has a smaller charge density, thus reducing its contribution to the stray field energy. The Néel tail is determined by using a balance between the stray field energy (K_d) and the anisotropy energy [18] and is given as $0.56tK_d/K$, where t is the film thickness and K_d can be determined from the saturation magnetization [18]. From this, we obtain $\delta_{tail} = 1.7$ μm for each tail. This estimate implies that the effective DW thickness can be significantly larger than δ and may fill the difference between δ and δ_W. Finally, we note that a negative DWR resistance has been observed in Fe, Ni, and Fe-Ni alloys [7–9]. These results together with the present ones suggest that an additional negative DWR, other than the AMR effect, may exist and that the negative DWR might be an intrinsic property uniquely associated with the DWs of Fe and Ni metals and alloys.

IV. CONCLUSION

We employed simultaneous measurements of the MR and the domain patterns in analyzing the origin of the MR change. We observed negative domain wall resistance in permalloy thin films when the domain wall was

nucleated. A direct mapping of the MR to the domain patterns enabled us to estimate the domain wall thickness; however, the estimate of the DW thickness based on the AMR effect turned out to be too large compared to the theoretical values, indicating that the observed domain wall resistance has possible origins other than the AMR effect. Further refinement of this method will be very useful in investigating the details of domain dynamics in ferromagnetic and multiferroic materials.

ACKNOWLEDGMENTS

This work was supported by the Yeungnam University Grant in 2007.

REFERENCES

[1] C. H. Marrows, Adv. Phys. **54**, 585 (2005).
[2] P. M. Levy and S. Zhang, Phys. Rev. Lett. **79**, 5110 (1997).
[3] G. Tatara and H. Fukuyama, Phys. Rev. Lett. **78**, 3773 (1997).
[4] R. McGuire and R. I. Potter, IEEE Trans. Magn. **MAG-11**, 1018 (1975).
[5] C. Hassel, M. Brands, F. Y. Lo, A. D. Wieck and G. Dumpich, Phys. Rev. Lett. **97**, 226805 (2006).
[6] R. Danneau, P. Warin, J. P. Attane, I. Petej, C. Beigne, C. Fermon, O. Klein, A. Marty, F. Ott, Y. Samson and M. Viret, Phys. Rev. Lett. **88**, 157201 (2002).
[7] U. Ruedinger, J. Yu, S. Zhang, A. D. Kent and S. S. P. Parkin, Phys. Rev. Lett. **80**, 5639 (1998).
[8] K. Hong and N. Giordano, J. Phys.: Condens. Matter **10**, L401 (1998).
[9] N. Giordano and B. Cetin, Phys. Stat. Sol. (b) **241**, 2404 (2004).
[10] U. Ebels, A. Radulescu, Y. Henry, L. Piraux and K. Ounadjela, Phys. Rev. Lett. **84**, 983 (2000).
[11] M. Viret, Y. Samson, P. Warin, A. Marty, F. Ott, E. Sondergard, O. Klein and C. Fermon, Phys. Rev. Lett. **85**, 3962 (2000).
[12] U. Rudiger, J. Yu, S. S. P. Parkin and A. D. Kent, J. Magn. Magn. Mater. **198-199**, 261 (1999).
[13] O'Handley, *Modern Magnetic Materials* (Wiley, New York, 2000).
[14] S. K. Decker and C. Tsang, IEEE Trans. Magn. **MAG-16**, 643 (1980).
[15] D. H. Kim, T. J. Hwang, K. S. Ryu and S. C. Shin, Phys. Stat. Sol. (c) **5**, 405 (2008).
[16] A. Hubert, IEEE Trans. Magn. **MAG-15**, 1251 (1979).
[17] A. Berger and H. P. Oepen, Phys. Rev. B **45**, 12596 (1992).
[18] A. Hubert and R. Schafer, *Magnetic Domains* (Springer, Berlin; New York, 1998).